Online parameter identification and state of charge estimation of lithium-ion batteries based on improved artificial fish swarms forgetting factor least squares and differential evolution extended Kalman filter.

XIAO, W., WANG, S., YU, C., YANG, X., QIU, J. and FERNANDEZ, C.

2022

Online Parameter Identification and State of Charge Estimation of Lithium-Ion Batteries Based on Improved Artificial Fish Swarms Forgetting Factor Least Squares and Differential Evolution Extended Kalman Filter

Weijia Xiao,[1,2,z] Shunli Wang,[1,2] Chunmei Yu,[1] Xiao Yang,[1,2] Jingsong Qiu,[1,2] and Carlos Fernandez[3]

[1]School of Information Engineering, Southwest University of Science and Technology, Mianyang 621010, China

[2]College of Electrical Engineering, Sichuan University, Chengdu 610065, China

[3]School of Pharmacy and Life Sciences, Robert Gordon University, Aberdeen AB10-7GJ, UK

Abstract: State of Charge (SOC) estimation is the focus of battery management systems, and it is critical to accurately estimate battery SOC in complex operating environments. To weaken the impact of unreasonable forgetting factor values on parameter estimation accuracy, an artificial fish swarm (AFS) strategy is introduced to optimize the forgetting factor of forgetting factor least squares (FFRLS) and to model the lithium-ion battery using a first-order RC model. A new method AFS-FFRLS is proposed for online parameter identification of the first-order RC model. In SOC estimation, it is not reasonable to fix the process noise covariance, and the differential evolution (DE) algorithm is combined with the extended Kalman filter (EKF) algorithm to achieve dynamic adjustment of the process noise covariance. A joint algorithm named AFS-FFRLS-DEEKF is proposed to estimate the SOC. to verify the reasonableness of the proposed algorithm, experiments are conducted under HPPC, BBDST and DST conditions, and the average errors of the joint algorithm under the three conditions are 1.9%, 2.7% and 2.4%, respectively. The validation results show that the joint algorithm improves the accuracy of SOC estimation.

1 Introduction

Since the last decade, electric vehicles (EVs) have rapidly developed and become widely used worldwide due to environmental pollution and the global energy crisis, which has attracted a great deal of attention [1]. Among them, the choice of batteries is extremely important, and lithium-ion batteries are the most widely used and promising batteries because of their long cycle life, good safety performance and high energy density [[2], [3], [4]]. State of Charge (SOC) estimation is one of the most important issues for Lithium-ion battery, and SOC represents the predicted value of the remaining energy of the battery [5], which cannot be obtained directly by measurement and is generally estimated by voltage and current measurements. In addition, other factors such as ambient temperature and noise can also affect the SOC value [6]. Therefore, for battery management systems (BMS), accurate estimation of SOC is critical but challenging at the same time.

Numerous research works have investigated on SOC estimation using various methods. One of them is the ampere-time integration method, which is a simple classical SOC estimation method. The ampere-time integration method calculates the total power flowing into and out of the battery by integrating the time and currently based on certain external characteristics of the system, such as current, time, and temperature compensation, to estimate the state of charge of the battery. Although the method is simple and reliable, the

error accumulation and current acquisition accuracy have a large impact on the accuracy of the calculation results [7].

Abundant studies have demonstrated that the SOC can be calculated from its mapping relationship to the open circuit voltage (OCV) [8, 9]. Based on the simulation model of a lithium battery, a model parameter update method based on the dynamic matrix control (DMC) algorithm is proposed to identify the OCV online and optimize the output to a predetermined trajectory through feedback correction and rolling for current and future input control [10]. In another paper [11], a temperature-based fractional-order RC circuit model was developed that uses an ambient temperature lookup table for OCV-SOC-T and a temperature-based offset function that facilitates the reduction of offsets due to model inaccuracies and operating conditions. However, the accuracy of SOC estimation using OCV-SOC mapping can be affected by driving style, ambient temperature, battery aging, and other factors [12]. Considering these factors, it is difficult to obtain an accurate OCV-SOC relationship. There is a potential relationship between impedance and SOC. The information measurement method of electrochemical impedance spectroscopy (EIS) is used to extract the EIS impedance features that are highly correlated with SOC and to establish a mapping relationship between impedance and SOC to estimate SOC [13]. However. Battery aging can affect the accuracy of impedance online measurements [14]. In addition, the internal temperature of the battery may also lead to changes in impedance and SOC [15].

Currently, data-driven methods are also heavily applied to SOC estimation, such as deep learning [16], neural networks [17], support vector machines [18], and long-short memory [19], which are usually based on data-driven methods. Data-driven is to build models that fit reality by training on large data sets [20]. However, using mixed data sets leads to poor model accuracy, and if only a single data set is used, it leads to poor model stability and generalization. To address these problems, a new multimodal integrated support vector regression (ME-SVR) method is proposed to estimate SOC by dividing the initial data into multiple subsets and building support vector machine models separately [21].

Kalman filter is the most commonly used method for SOC estimation, such as extended Kalman filter [22, 23], untraced Kalman filter [24, 25], cubature Kalman filter [26, 27], central difference Kalman filter [28], linear Kalman filter [29], etc. The Kalman filter is an optimal linear state estimation method that uses a recursive approach to solve linear filtering problems [30]. However, the validity of EKF estimation can be affected due to factors such as model parameters, uncertainty of noise covariance, etc. An adaptive tracking EKF (ATEKF) SOC estimation method for adaptive correction of error covariance is proposed [31]. In a series of SOC estimation methods with Kalman filter, observation noise is one of the key factors affecting the estimation results, and a multi-innovation cubature Kalman filter (MICKF) algorithm, combined with a robust fuzzy model, is proposed to effectively filter the noise in the observation [24]. Process noise not only leads to divergence of SOC estimation results but also causes hysteresis phenomena. In this work, literature

[32] considers the effect of hysteresis on SoC estimation and applies a differential evolution based SoC estimation technique to accurately estimate SoC while minimizing the hysteresis effect. The literature [33] proposes a regression algorithm with differential evolution to represent polynomials of SOC-related parameters, Gaussians, and parameters of sine and exponential equations as a function of SOC, reducing the memory footprint. In summary, EKF remedies the defects of Kalman filtering and can obtain optimal solutions to local problems, but it is affected by process noise, and the differential evolution algorithm is flexible enough to be used for optimization in different fields. Therefore, it is feasible to combine the DE algorithm with the EKF algorithm to adaptively optimize the process noise variance and make up for the shortcomings of the EKF algorithm.

Based on the above methods, this paper proposes a joint artificial fish swarm optimized forgetting factor least squares-differential evolutionary extended Kalman filter (AFS-FFRLS-DEEKF) algorithm to estimate the SOC of lithium battery. Firstly, a first-order RC model is established to describe the dynamic characteristics of the battery. In the FFRLS algorithm, an artificial fish swarm strategy is introduced to optimize the forgetting factor for the value of forgetting factor and an optimization objective function is established with the objective of minimizing the end voltage, and an online parameter identification method based on the AFS-FFRLS algorithm is proposed to optimize the forgetting factor and make it dynamic. Secondly, the differential evolution (DE) algorithm is combined with the extended Kalman filter (EKF) to achieve dynamic adjustment of the process noise covariance, and a DEEKF algorithm is proposed to estimate the SOC. Finally, to prove the effectiveness of the proposed algorithm, the end voltage estimation results of AFS-FFRLS and FFRLS are compared in the parameter identification section, and the joint algorithm AFS-FFRLS-DEEKF is synthesized and compared with several other algorithms in the SOC estimation section.

The innovation points of this paper are described as follows.

(1) The artificial fish swarm algorithm is proposed to combine with the FFRLS algorithm to optimize the forgetting factor of FFRLS, make it dynamic, reduce the influence brought by unreasonable forgetting factor values, solve the local extremum problem of FFRLS algorithm, obtain the global extremum, improve the parameter identification accuracy, and lay the foundation for the subsequent SOC estimation.

(2) The DEEKF algorithm is proposed to realize the adaptive adjustment of process noise covariance, optimize the unreasonable problem of fixed process noise covariance of the EKF algorithm, and improve the accuracy of SOC estimation under the logic of real-time changes of actual noise.

The rest of the paper is structured as follows: Section 2 establishes the first-order RC model and describes the newly proposed AFS-FFRLS algorithm and the DEEKF algorithm in detail. Section 3 conducts a comprehensive experiment on parameter identification and SOC estimation to verify the effectiveness of the new algorithms. Finally, Section 4 concludes the whole work.

2 Theoretical analysis

This section provides a comprehensive description of mainly two newly proposed algorithms. Section 2.1 establishes the first-order RC equivalent model and describes Kirchhoff's law equations as well as the discretized spatial equations. Section 2.2 describes the FFRLS algorithm. Section 2.3 describes the parameter identification method AFS-FFRLS algorithm in this paper. Section 2.4 gives the theoretical analysis of the DEEKF algorithm for estimating the SOC.

2.1 First-order RC equivalent circuit modeling

The first-order RC equivalent model can accurately simulate the characteristics of lithium-ion batteries with a reasonable amount of computational control. It consists of an ideal current source, an internal resistance R_0 and an RC network. Where the RC network consists of a resistor and a capacitor, which used to describe the dynamics of the battery. The constructed first-order model is shown in Figure 1.

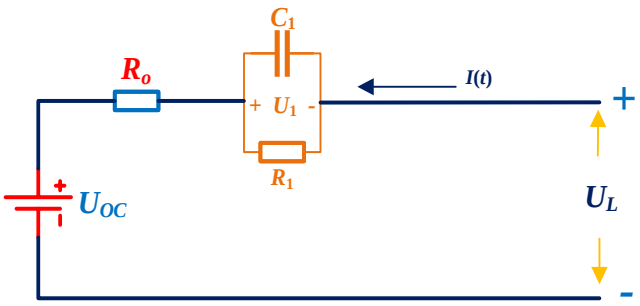

Figure 1. First-order RC equivalent model

In Figure 1, U_{oc} represents the open-circuit voltage, R_0 is the internal resistance of the battery, R_1 is the polarization resistor, C_1 is the polarization capacitor, loop R_1C_1 characterizes the process of rapid changes in circuit voltage, U_L is the battery terminal voltage. Defining the orientation of discharge as positive, the KVL equation of the circuit file is shown in Equation (1).

$$\begin{cases} U_L = U_{oc} - IR_0 - U_1 - U_2 \\ \dfrac{dU_1}{dt} = \dfrac{1}{C_1} - \dfrac{U_1}{R_1C_1} \end{cases} \tag{2}$$

In Equation (3), U_1 indicates the terminal voltages of the sRC circuit, and U_{oc} represents open-circuit voltage which can be expressed as a function of SOC, where x_k=[SOC_k, U_{1k}] is the state variable, and spatial state expressions of the model shown in Equation (4) can be obtained after discretizing Equation (5).

$$\begin{cases} \begin{bmatrix} SOC_k \\ U_{1,k} \end{bmatrix} = \begin{bmatrix} 1 & 0 \\ 0 & e^{\frac{\Delta t}{\tau_1}} \end{bmatrix} \begin{bmatrix} SOC_{k-1} \\ U_{1,k-1} \end{bmatrix} + \begin{bmatrix} \frac{\eta \Delta t}{Q_N} \\ R_1\left(1-e^{\frac{\Delta t}{\tau_1}}\right) \end{bmatrix} I(t)_k + w_k \\ U_{L,k} = U_{OC}(SOC_k) + U_{1,k} + I(t)_k R_{0,k} + v_k \end{cases} \tag{6}$$

In Equation (7), the two equations are the state and viewing equations of the system, separately. The Δt represents the sampling time, the time constant is denoted by τ, $\tau_1=R_1C_1$, the subscripts k and k-1 represent the current and previous moment state respectively. W_k represents the observation error, V_k is the measurement error, Q_N indicates rated capacity of the battery, η represents the Coulomb efficiency, and the general value is 1.

2.2 Forgetting factor least squares

Theoretically, the more data collected by parameter identification, the higher the accuracy of parameter estimation, but too much data can easily lead to data saturation, which in turn leads to less information obtained by the algorithm from new data [34]. Due to the phenomenon of "filter saturation" in the least-squares method [35], meaning that the values of the gain K and the system covariance P become smaller and smaller as the number of data iterations of the algorithm increases. As a result, the algorithm's ability to correct the data gradually decreases and data saturation increases, which eventually leads to an increase in parameter identification errors. Therefore, the forgetting factor recursive least squares (FFRLS) method is formed [36, 37]. The role of the forgetting factor is to give less weight to the long-running data in the recognition process while the latest observation data occupies more weight. The relationship between the parameters and the terminal voltage is expressed as a linear equation, as shown in Equation (8).

$$y = x^T u + e \tag{8}$$

where y is the measured value of the system output. x is the state output vector, its elements can consist of parameters or expressions of parameters. u is the system input vector, consisting of the system measurement signals. e is the sampling error of the sensor.

According to the system transfer function, a linear regression model of the battery parameters and terminal voltage is derived, as shown in Equation (4).

$$\begin{cases} U_{L,k} = \theta_k^T \varphi_k \\ \theta_k = \left[\theta_{1,k} \;\; \theta_{2,k} \;\; \theta_{3,k}\right]^T \\ \varphi_k = \left[U_{L,k-1} \;\; 1 \;\; I_{t,k} \;\; I_{t,k-1}\right]^T \end{cases} \tag{9}$$

where φ_k is the input vector. θ_k is the output vector. $\theta_{i,k}$ is the expression of the cell parameters.

The FFRLS algorithm introduces a forgetting factor λ to adjust new and old data weights, and λ takes a value close to 1, which is generally taken as $0.95 \le \lambda \le 1.00$. Setting the gain coefficient as $K(k)$, the parameter vector as $\theta(k)$, and the covariance matrix as $P(k)$, the FFRLS Equation is shown in Equation (10).

$$\begin{cases} K(k) = P(k-1)\varphi(k)\left[\lambda + \varphi^T(k)P(k-1)\varphi(k)\right]^{-1} \\ \hat{\theta}(k) = \hat{\theta}(k-1) + K(k)\left[y(k) - \varphi^T(k)\hat{\theta}(k-1)\right] \\ P(k) = \frac{1}{\lambda}\left[E - K(k)\varphi^T(k)\right]P(k-1) \end{cases} \tag{10}$$

2.3 Forgetful factor least squares for artificial fish swarm optimization

Although the FFRLS algorithm can weaken the effect of aged data and deal with the data saturation problem to some extent [38], the recognition effect of FFRLS algorithm mainly depends on the value of λ. If the value of λ is smaller, the tracking ability is stronger, but the result tends to fluctuate. If the value of λ is larger, the stability is stronger, but the tracking ability is weaker. To weaken the influence of the λ-value problem, the AFS algorithm is proposed to optimize the forgetting factor λ, which minimizes the terminal voltage error. The behavioral functions of the AFS algorithm are defined as functions such as foraging, clustering, tail-chasing, and random. The model expression for the artificial fish population is shown in Equation (11).

$$\begin{cases} X_V = X + Visuanl * Rand() \\ X_{next} = X + \frac{X_V - X}{\left\| X_V - X \right\|} * Step * Rand() \end{cases} \tag{11}$$

Where X is the initial position of the artificial fish, X_V is a position within the current field of view of the artificial fish, and X_{next} is the position of the next state of the artificial fish. *Step* denotes the step size, and *Rand* () denotes the random function that generates a random number between 0 and 1.

At first, the artificial fish performs foraging behavior. The artificial fish X_i randomly selects a state X_j within its field of view, and the expression of X_j is shown in Equation (12).

$$X_j = X_i + Visuanl * Rand() \tag{12}$$

The values of objective functions Y_i and Y_j are calculated for X_i and X_j, respectively, and if Y_j is better than Y_i, X_i is moved one step in the direction of X_j, $X_i = (\lambda_1, \lambda_2, \ldots, \lambda_i)$. This process is shown in Equation (13).

$$X_i^{t+1} = X_i^t + \frac{X_j - X_i^t}{\left\| X_j - X_i^t \right\|} * Step * Rand() \tag{13}$$

To obtain a new central position, the artificial fish will perform clustering behavior, and this process is shown in the expression of Equation 9.

$$X_i^{t+1} = X_i^t + \frac{X_c - X_i^t}{\left\| X_c - X_i^t \right\|} * Step * Rand(),\ Y_c / n_f > \delta Y_i \tag{14}$$

where X_C is the center location, n_f is the number of partners, and δ denotes the congestion factor.

The artificial fish searches for the functionally optimal partner among the partners in the current field of view, it performs the tailing behavior, and the process is shown in Equation 10.

$$X_i^{t+1} = X_i^j + \frac{X_j - X_i^t}{\left\| X_j - X_i^t \right\|} * Step * Rand(),\ Y_j / n_f > \delta Y_i \tag{15}$$

The δ deals with the minimal value problem and performs foraging behavior if the conditions in Equation (14) and (15) are not satisfied. The δ expression is shown in Equation (16).

$$\delta = \alpha n_{\max},\ \alpha \in (0,1] \tag{16}$$

where α is the extreme proximity level and n_{max} is the maximum number of artificial fish expected to aggregate in the neighborhood.

Random behavior is a default behavior of foraging behavior, where artificial fish move one step randomly to reach a new state, as shown in Equation (17).

$$X_i^{t+1} = X_i^t + Visuanl * Rand() \tag{17}$$

With the minimum terminal voltage error as the optimization objective, the AFS algorithm is introduced to optimize the forgetting factor in real-time to improve the accuracy of online identification. Combining Equation (10), the fitness function is determined as Equation (18).

$$f = \left| U_L(k) - U_{OC}(k) - \varphi^T(k)\hat{\theta}(k-1) \right| \tag{18}$$

The expression for the estimated value of the system of θ_k optimized by the artificial fish population is shown in Equation (19).

$$\hat{\theta}_k = \hat{\theta}_{k-1} + \frac{P(k)\varphi(k+1)\left[y(k+1) - \varphi^T(k+1)\hat{\theta}_{k-1} \right]}{\left[\lambda_i^k + \varphi^T(k+1)P(k)\varphi(k+1) \right]} \tag{19}$$

With the identified results of θ_k, the parameters can be further calculated according to Equation (5). The calculation equation is shown in Equation (20).

$$\begin{cases} R_{0,k} = \dfrac{\hat{\theta}_{2,k} - \hat{\theta}_{3,k}}{1 + \hat{\theta}_{1,k}} \\ R_{1,k} = \dfrac{T + (-1 - \hat{\theta}_{1,k}) \cdot T \cdot 2T}{(\hat{\theta}_{1,k} - 1)(\hat{\theta}_{2,k} + \hat{\theta}_{3,k})} - R_{0,k} \\ C_{1,k} = \dfrac{1}{2} \cdot \dfrac{T \cdot (\hat{\theta}_{1,k} + 1) \cdot R_{1,k}}{1 - \hat{\theta}_{1,k}} \\ \tau = R_{1,k} C_{1,k} \end{cases} \tag{20}$$

In summary, the flow of the AFS-FFRLS algorithm is shown in Figure 2.

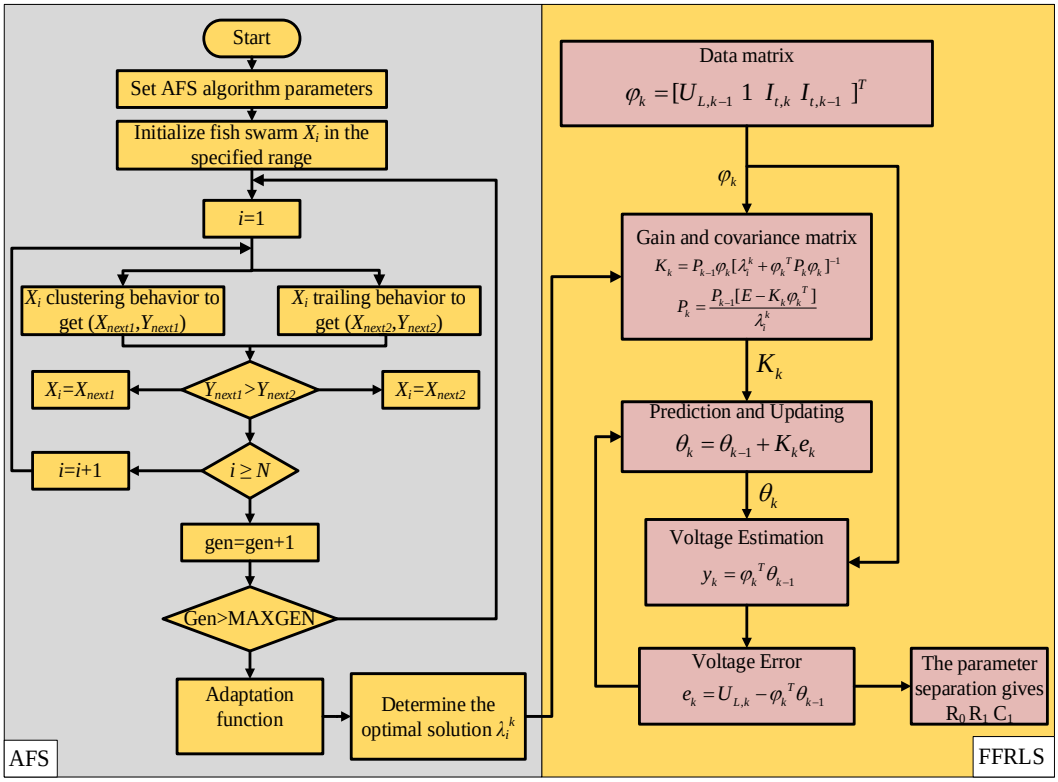

Figure 2. Flow chart of AFS-FFRLS algorithm

2.4 Differential Evolution Extended Kalman Filter Algorithm

Due to the complex and variable working environment, the parameters of the equivalent model are greatly influenced by the environment, leading to a decrease in the estimation accuracy of the SOC. In traditional EKF algorithm, the observed noise variance Q_k will affect the SOC estimation result [39]. The Q_k value is generally a set of fixed values, which is difficult to obtain accurately in practical application models, and the noise is unmeasurable and variable [40-42], and it is not reasonable to fix the process noise variance, so the differential evolution (DE) algorithm is introduced to optimize the process noise variance fixed in the original extended Kalman algorithm. So that the variance of noise can be automatically revised based on the changes in the environment, with this constant, the changed optimal variance is substituted into the original algorithm to complete the online estimation of SOC under cycle conditions. The flow of the DE algorithm is described as follows.

1) System initialization

$$\begin{cases} \hat{x}_0^+ = E(x_0) \\ p_0^+ = E\left[(x_0-\hat{x}_0^+)(x_0-\hat{x}_0^+)^T\right] \end{cases} \tag{21}$$

2) Update of the state variable

$$x_{k|k-1} = A_{k-1}x_{k-1} + B_{k-1}I_{k-1} \tag{22}$$

In Equation (22), A represents the state transition matrix, and B is the control matrix.

3) Update of the system prior covariance

$$P_{k|k-1} = A_{k-1}P_{k-1}A_{k-1}^{T} + Q_{k-1} \tag{23}$$

In Equation (23), Q_{k-1} is the noise variance at time k-1. If the process noise Q_{k-1} is not fixed and changes with the filter, the DE algorithm is used to obtain its variance according to the process noise at different times, and select the optimal solution from Q_0 to Q_k.

4) Population initialization

$$\begin{cases} x_{i,k}(0) = l_k + rand() * (u_k - l_k) \\ k = 1, 2, ..., d,\ i = 1, 2, ..., N \end{cases} \tag{24}$$

In Equation (24), *rand* () is a random number uniformly distributed between 0 and 1, u_k and l_k are the upper and lower bounds of the search, and Q_k, Q_0 are the upper and lower bounds respectively.

5) Mutation operation

$$x_i(g) = x_{r1}(g) + F * \left[x_{r2}(g) - x_{r3}(g) \right] \tag{25}$$

In Equation (25), $Q_i(g)$ is a variant individual, F is the compression scale factor, which ranges from 0 to 1, x_{r1}, x_{r2} and x_{r3} are the three parents.

6) Crossover operation

The crossover operation retains the better variables and adopts the binomial crossover method. The implementation of the binomial crossover method is shown in Equation (26).

$$y_{i,g}(g) = \begin{cases} X_{i,g}(g), r < cr \ \ or \ \ j = rnd \\ x_{i,g}(g), \ others \end{cases} \tag{26}$$

Where r is a uniformly spread random number between 0 and 1 generated by each variable, cr is the crossover probability of the variable and rnd is an evenly spread integer between 1 and d. If $r<cr$, accept the component corresponding to the target individual, otherwise keep the component corresponding to the current individual.

7) Select action

The standard differential evolution algorithm adopts a greedy selection method, and the operations are shown in Equation (27).

$$x_i(g+1) = \begin{cases} X_i(g), f\left[X_i(g)\right] < f\left[x_i(g)\right] \\ x_i(g), \ others \end{cases} \tag{27}$$

In Equation (27), this optimal solution is assigned to Q_i to be applied to the next filtering, and the greedy selection method improves the population performance and gradually approaches the optimal solution.

8) Update of Kalman gain

$$K_k = P_{k|k-1}C_k^{T}\left(C_k P_{k|k-1} C_k^{T} + R_k\right)^{-1} \tag{28}$$

In Equation (28), P is the error covariance matrix, C is the observation matrix, and R_k is the observation noise variance.

9) State posterior estimation

$$\hat{x}_{k|k} = x_{k|k-1} + K_k \left[Y_k - y_k \right] \tag{29}$$

In Equation (29), Y_k-y_k represents the innovation at the current moment.

10) Update of the error covariance

$$\hat{P}_{k|k} = \left(E - K_k C_k \right) P_k \tag{30}$$

In Equation (30), E represents the identity matrix.

In summary, the process of estimating SOC based on AFS-FFRLS and DEEKF algorithm is shown in Figure 3.

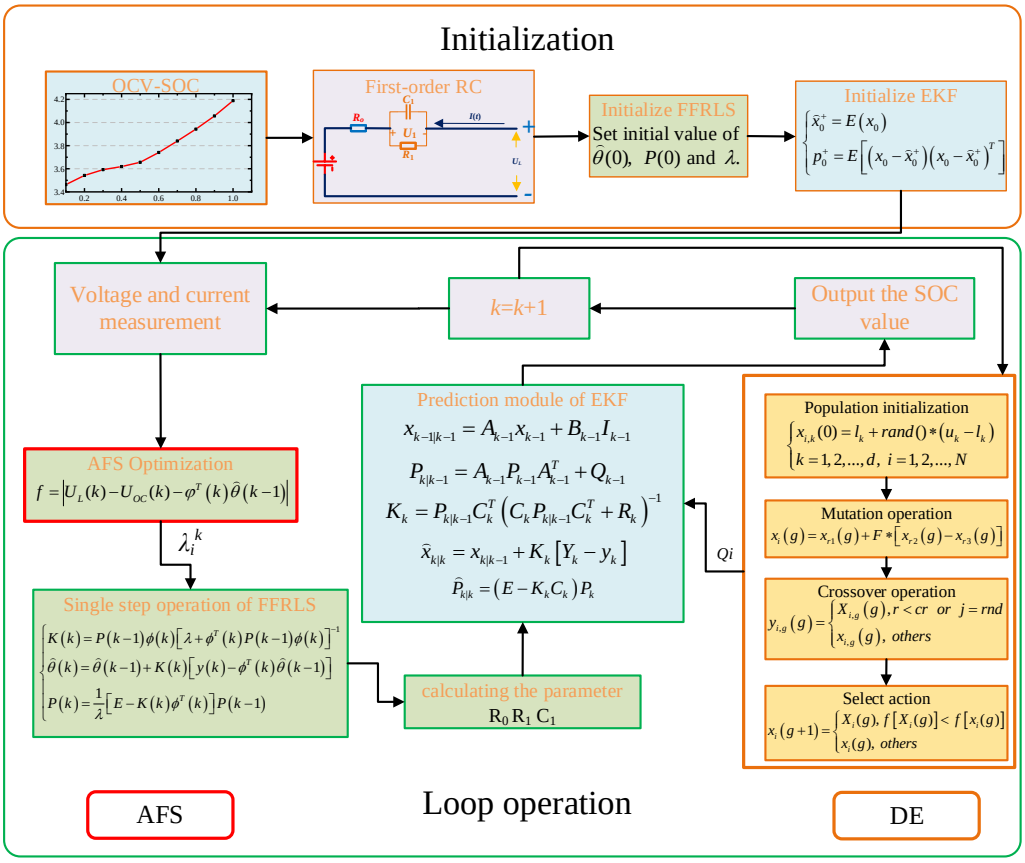

Figure 3. Flow chart of SOC estimation

In Figure 3, the introduction of the differential evolution algorithm optimizes the variance of the process noise and improves the accuracy of the entire Kalman algorithm. Using the AFS-FFRLS algorithm for parameter identification also improves the model parameter identification accuracy to a certain extent, laying a foundation for improving the SOC estimation accuracy of lithium-ion battery.

3 Analysis of experimental results

This section reports the experimental validation results of the parameter identification module and the SOC estimation module. Section 3.1 gives the identification results for each parameter and the terminal voltage estimation results for the three operating conditions. Sections 3.2, 3.3, and 3.4 perform SOC estimation based on the joint AFS-FFRLS-DEEKF algorithm for HPPC, BBDST, and DST operating

conditions, respectively, and compare with various joint algorithms. Section **Error! Reference source not found.** performs SOC estimation under three operating conditions at an initial value of SOC of 0.8.

The ternary lithium-ion battery is the object of study, the rated capacity of the battery is 70 Ah, and the actual capacity is 68.47 Ah. The experimental stage is built with the BTS200-100-104 battery testing equipment and temperature control box provided by Shenzhen Yakeyuan Technology Co. The battery is charged and discharged under constant temperature (25°C) to obtain relevant experimental data. The experimental platform is shown in Figure 4.

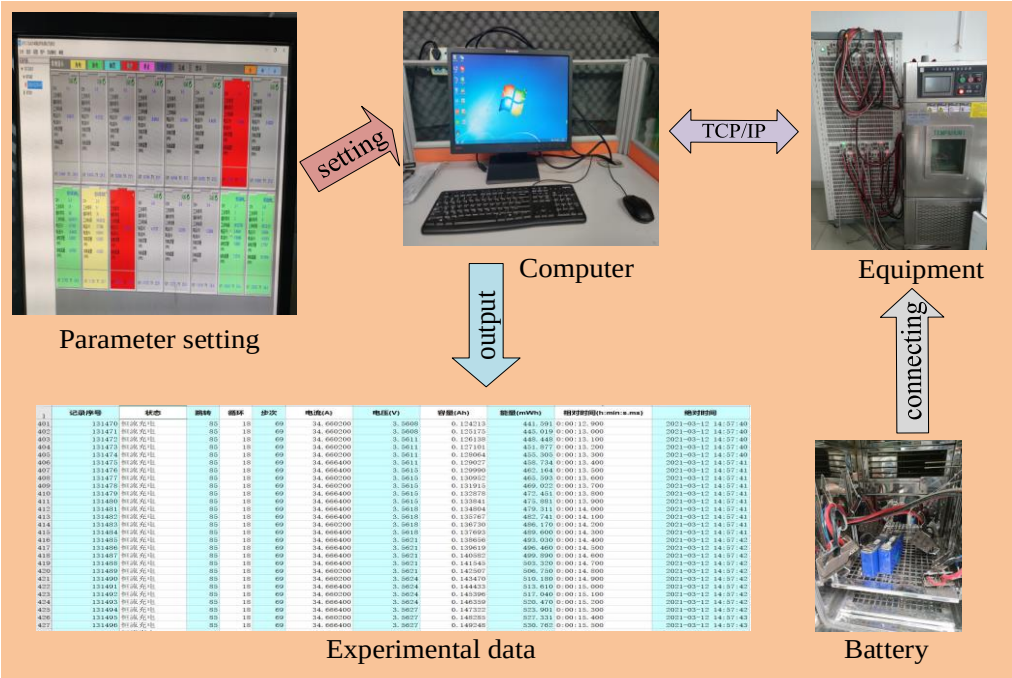

Figure 4. Experimental platform

3.1 Parameter identification results and terminal voltage prediction

Taking the HPPC condition as the condition of parameter identification experiment, the parameters of the first-order RC model are identified online according to the AFS-FFRLS algorithm flow, and the identification results are compared with those of RLS and FFRLS algorithms, to verify the feasibility of the AFS-FFRLS algorithm. The parameter identification results of different algorithms are shown in Figure 5.

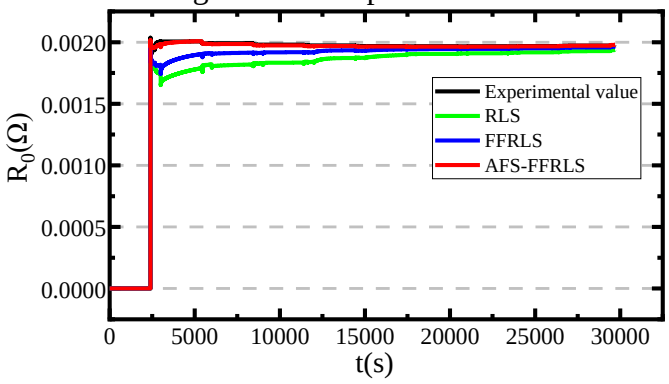

(a) Identification results of R_0

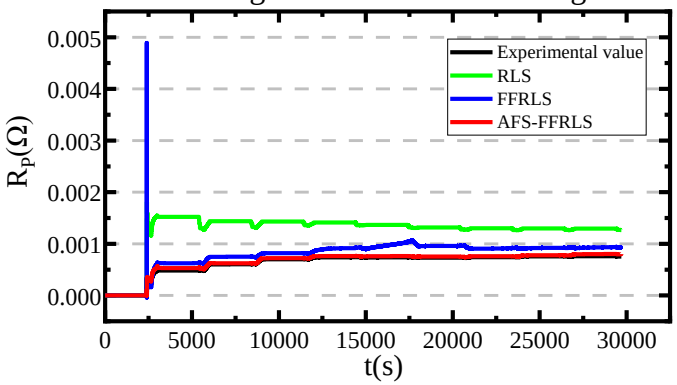

(b) Identification results of R_P

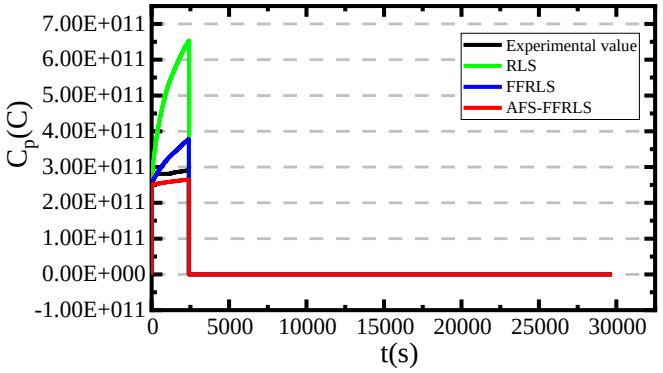

(c) Identification results of C_P

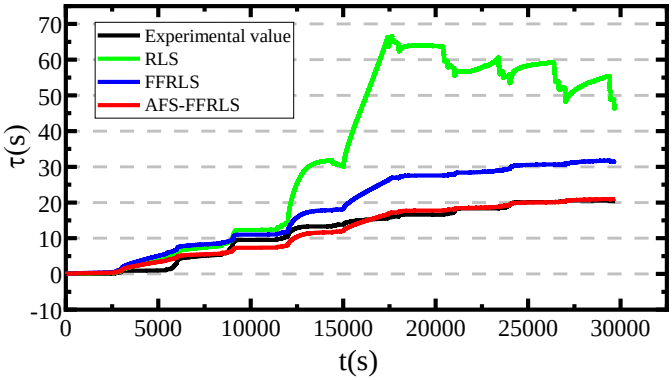

(d) Identification results of τ

Figure 5. Parameter identification results

In Figure 5, the experimental data values of each parameter are used as a reference. It can be seen that the results of the RLS algorithm deviate from the reference throughout the identification process, and the results of τ fluctuate drastically, showing poor convergence. After adding the forgetting factor (λ=0.98), the recognition accuracy of the FFRLS algorithm has been improved and the convergence in the whole parameter recognition process has been improved, but there is still some deviation from the reference. And the results of the proposed AFS-FFRLS algorithm show the best agreement with the reference, and the fluctuation range of tao also shows its better convergence, which verifies the effectiveness of the AFS-FFRLS algorithm.

To further verify the accuracy of the proposed algorithm in identifying the model parameters, end-voltage prediction experiments were conducted and error comparisons were made under HPPC, DST and BBDST operating conditions, as shown in Figure 6.

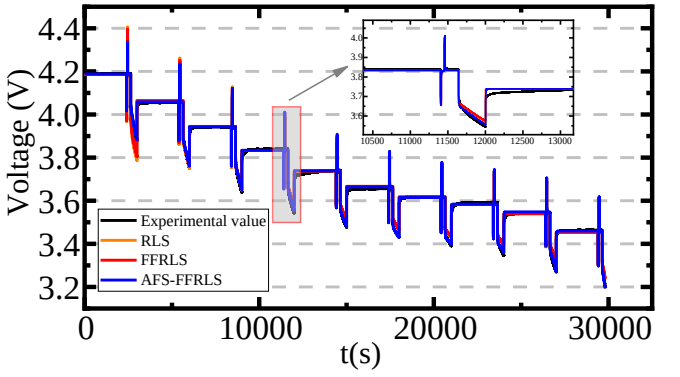

(a) Terminal voltage prediction results under HPPC working condition

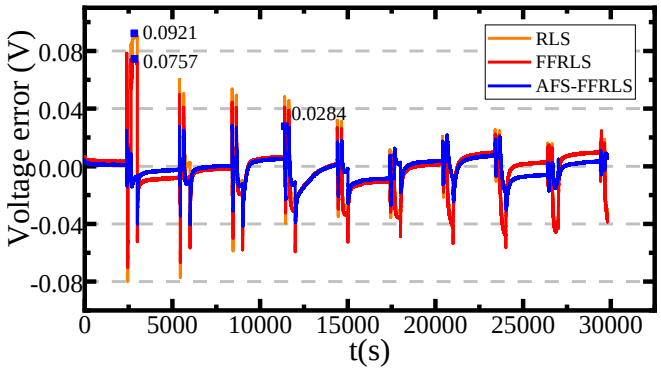

(b) Terminal voltage prediction error under HPPC working condition

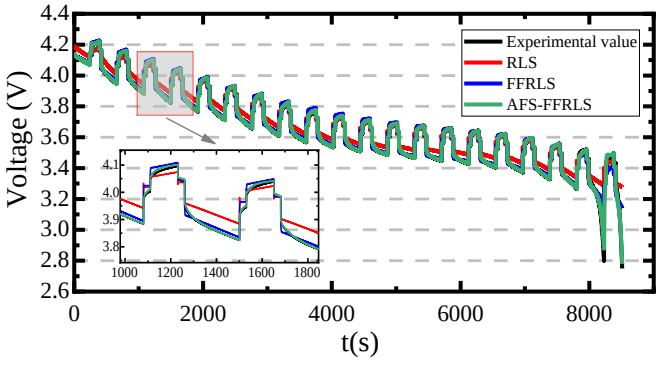

(c) Terminal voltage prediction results under DST working condition

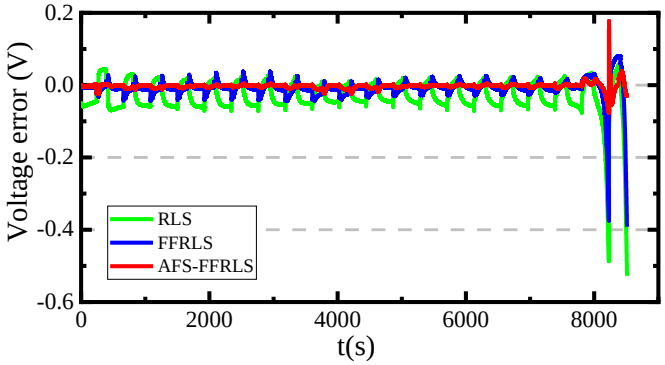

(d) Terminal voltage prediction error under DST working condition

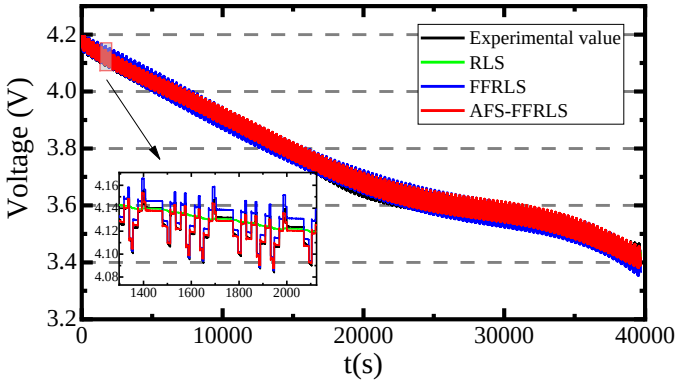

(e) Terminal voltage prediction results under BBDST working condition

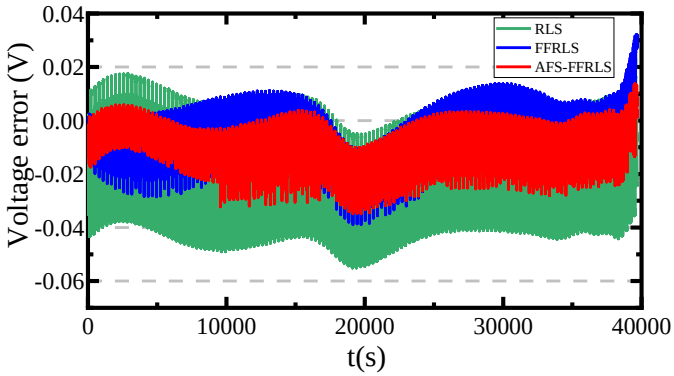

(f) Terminal voltage prediction error under BBDST working condition

Figure 6 Terminal voltage prediction results under different operating conditions

In Figure 6, it can be seen that the RLS algorithm has the worse terminal voltage prediction effect among the three algorithms for each operating condition, and there are obvious divergences and fluctuations throughout the simulation process. After adding the forgetting factor, the FFRLS algorithm reduces the estimation error, but there is still some discrepancy with the experimentally measured terminal voltage. By comparison, the AFS-FFRLS algorithm has the smallest simulation error and the best convergence among the three algorithms, and the highest affinity with the reference, which means that the AFS-FFRLS algorithm is a better choice among the online parameter identification methods for lithium-ion batteries.

3.2 Analysis of SOC estimation results under HPPC condition

The HPPC experiment includes charging and discharging of different durations and the shelving steps, which can better emulate the actual working scenario of the battery. The variance of process noise is optimized by the differential evolution algorithm, and setting the process noise covariance matrix Q to be a third-order diagonal matrix whose main diagonal is Y, where Y is the optimal solution selected by each iteration of the differential evolution algorithm, the observation noise covariance matrix R is set to 0.01, the actual SOC initial value is 1. The voltage and current under HPPC conditions are shown in Figure 7, and the estimation results and error comparisons of different algorithms are presented in Figure 8. In addition, the mean absolute error (MAE), maximum absolute error (MAX) and root mean square error (RMSE) of various algorithms are shown in Table 1.

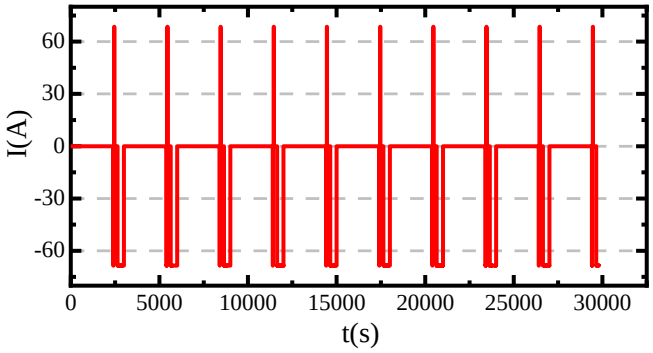

(a) Current

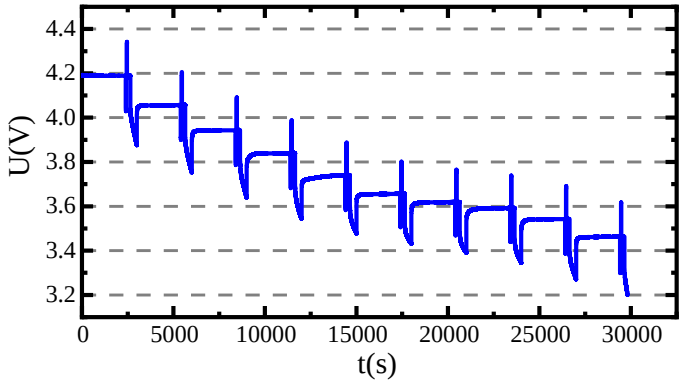

(b) Voltage

Figure 7 Voltage and current at HPPC operating conditions

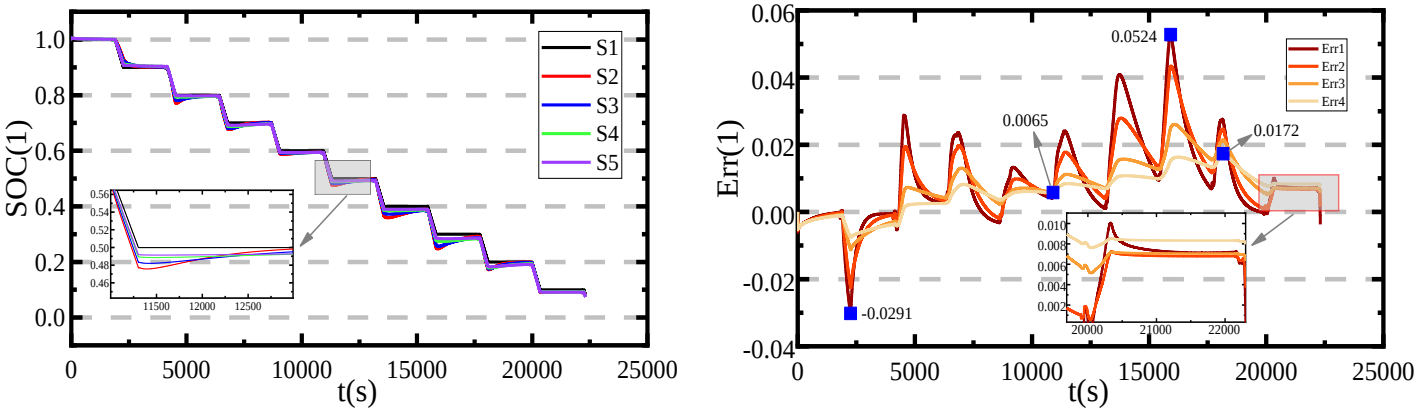

(a) SOC estimation results of different algorithms under HPPC conditions

(b) Error comparison of different algorithms under HPPC conditions

Figure 8. SOC estimation results and errors of HPPC condition

Table 1. Comparison of SOC estimation results of different algorithms under HPPC conditions

Method	MAE	MAX	RMSE
EKF	0.02351	0.05242	0.02517
FFRLS-EKF	0.02295	0.04343	0.02301
AFS-FFRLS-EKF	0.02151	0.02662	0.02133
AFS-FFRLS-DEEKF	0.01658	0.01729	0.01587

In Figure 8(a), S1 is the actual SOC value, S2 indicates the SOC result estimated by the EKF algorithm based on the second-order RC model, S3 represents the SOC result estimated by FFRLS and EKF algorithms, and S4 indicates the SOC estimated by the AFS-FFRLS and EKF algorithms as a result, S5 represents the SOC estimation result based on AFS-FFRLS and DE-EKF algorithm.

In Figure 8(b), Err2 and Err3 represent the SOC estimation errors of the FFRLS-EKF and AFS-FFRLS-EKF algorithms, respectively. It can be seen that the fluctuation range of the Err3 curve is significantly smaller than that of the Err2 curve, which proves that the online parameter identification method of AFS-FFRLS can further improve the SOC estimation accuracy compared with the FFRLS algorithm, and verifies the effectiveness of the optimization of the AFS algorithm. Err4 represents the error curve of the joint algorithm AFS-FFRLS-DEEKF, and compared with Err3 it can be seen that the DEEKF algorithm performs better in the case of the same AFS-FFRLS parameter identification method, which verifies the feasibility of dynamic optimization of process noise covariance.

Similarly, it can be seen from Table 1 that the joint algorithm AFS-FFRLS-DEEKF performs the best under all the three error metrics compared with the other three algorithms, and the disparity between the maximum absolute error (MAX) and MAE, RMSE is small, indicating that the AFS-FFRLS-DEEKF algorithm improves the convergence while improving the accuracy of SOC estimation, which verifies the feasibility of the joint algorithm.

3.3 Analysis of experimental results under BBDST condition

In the practical application environment of lithium-ion battery, the working conditions are complex and variable. To verify the stability and accuracy of the SOC prediction of the improved algorithm, BBDST experiments are performed on lithium-ion batteries and experimental data were collected. The BBDST working condition includes 19 steps including starting, coasting, acceleration, braking, and rapid acceleration of the pure electric bus, which can better restore the working status of lithium-ion batteries in real-life scenarios. The voltage and current for the BBDST condition are shown in Figure 9.

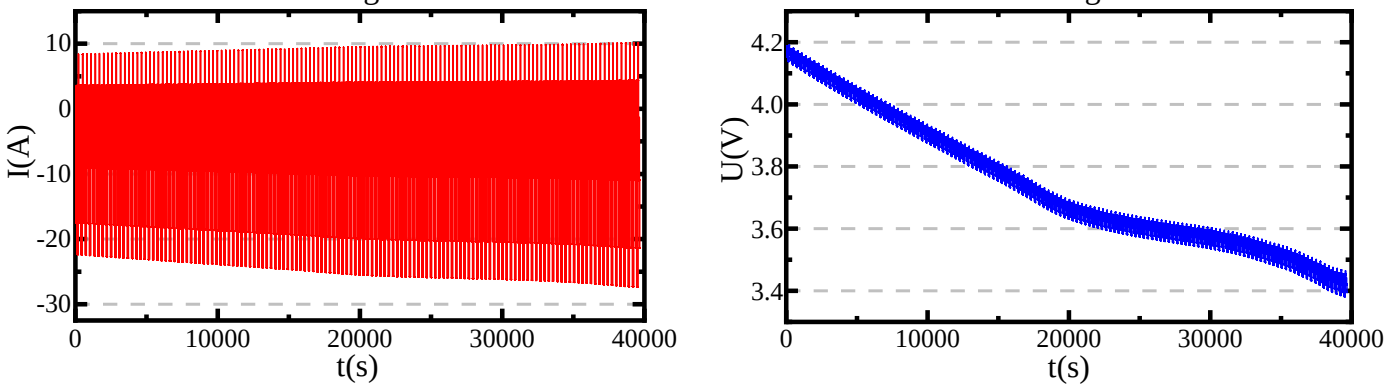

(a) Current (b) Voltage

Figure 9. Current and voltage test results under BBDST condition

To verify the effectiveness of the improved algorithm, SOC estimation is performed on the basis of the EKF, FFRLS-EKF, AFSFFRLS-EKF and AFSFFRLS-DEEKF algorithms respectively. The process noise covariance Q is set as a diagonal matrix with the main diagonal element equal to Y, where Y is the optimal solution selected by each iteration of the differential evolution algorithm, and the observation noise covariance R is set to 0.01, the actual SOC initial value is 1. The experimental verification results are shown in Figure 10.

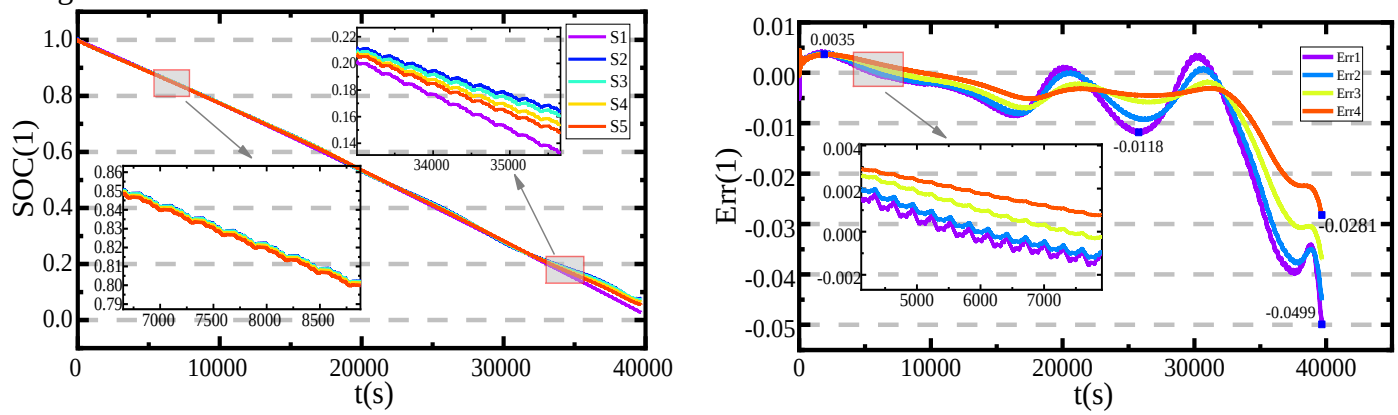

(a) SOC estimation results under BBDST conditions (b) Error of SOC estimationunder BBDST conditions

Figure 10. SOC estimation results under BBDST condition

Table 2. Comparison of SOC estimation results of different algorithms under BBDST conditions

Method	MAE	MAX	RMSE
EKF	0.04625	0.04992	0.04406
FFRLS-EKF	0.03474	0.04512	0.03303
AFS-FFRLS-EKF	0.02657	0.03698	0.03056
AFS-FFRLS-DEEKF	0.01356	0.02819	0.01795

In Figure 10(a), S1 indicates the actual SOC value, S2 is the SOC estimated result of the EKF algorithm based on the offline parameter identification, S3 indicates the SOC estimated resultof EKF algorithm based on the FFRLS parameter identification, and S4 represents the SOC estimated result based on AFS-FFRLS algorithm and the EKF algorithm. S5 represents the SOC estimation value based on the AFS-FFRLS algorithm and the DE-EKF algorithm.

In Figure 10(b), Err1, Err2, Err3, Err4, and Err5 are the SOC prediction errors matching with the S2~S5 algorithms in Figure 10(a) respectively. It can be seen that in the final stage of the experiment, different algorithms exhibit different degrees of divergence, which is caused by the violent chemical reactions occurring inside the battery at the end of the discharge. In Table 2, the joint algorithm AFS-FFRLS-DEEKF controls the MAE and RMSE indexes within 2% and the MAX index within 3%, indicating that the joint algorithm can still maintain the best performance under the more complex operating conditions, further verifying the effectiveness of the AFS-FFRLS-DEEKF algorithm.

3.4 Analysis of experimental results under DST condition

In actual application, the current reacted in real time of lithium-ion batteries is complex and changeable. Under different operating conditions, there are often abrupt swapping and stops of current, so it is not only necessary to strictly require the dynamic performance of the battery but also the SOC of the lithium-ion battery has to be estimated under complex operating conditions. To further validate the model for SOC estimation of lithium-ion batteries under more complex operating conditions, the self-defined Dynamic Stress Test (DST) working condition experimental data is used to simulate the model. In the meantime, the Ampere-hour integral method and EKF algorithm are added under the same working conditions to carry out the synchronous simulation. The experimental procedures of the DST are as follows:

(1) The battery is charged to a maximum terminal voltage of 4.20V with a constant current of 1C, followed by charging at a constant voltage until the current reduces to 0.05C.

(2) After charging is completed, the battery is put aside to maintain the battery voltage. The dwell time was chosen as 30 minutes due to the small capacity of the selected Lithium-ion battery.

(3) Discharging the battery at a constant current rate of 0.5C for 4 minutes and set aside for 30 seconds after stopping the discharge.

(4) The lithium-ion battery is charged with a constant current rate of 0.5C for 2 minutes. The battery is shelved for 30s after charging.

(5) The constant current discharge is performed at a rate of 1C for 4 minutes.

The voltage and current for DST condition are shown in Figure 11.

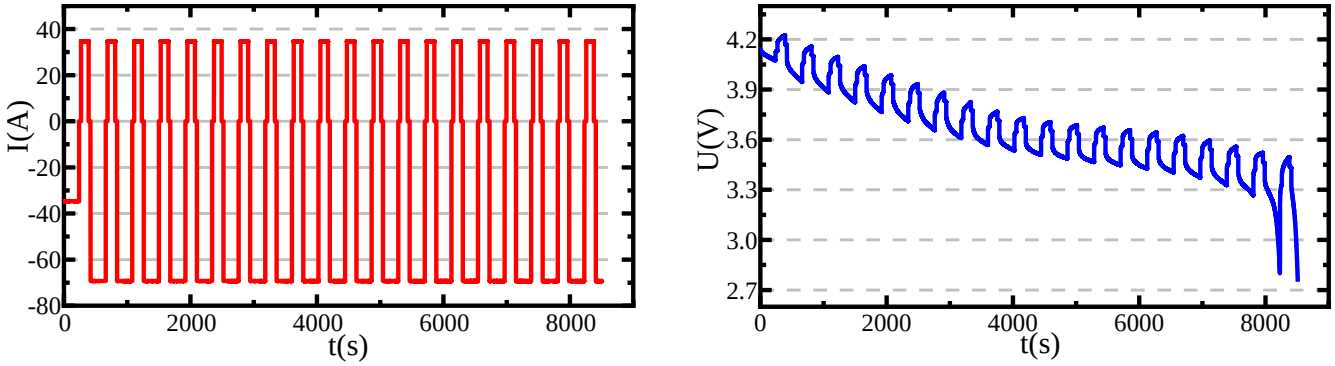

(a) Current (b) Terminal voltage

Figure 11. Current and voltage test results under DST condition

The process noise covariance Q is set as a diagonal matrix whose main diagonal element is equal to Y, where Y is the optimal solution selected by each iteration of the differential evolution algorithm, and the observation noise covariance R is set to 0.01, the actual SOC initial value set to 1. The experimental verification results are shown in Figure 12.

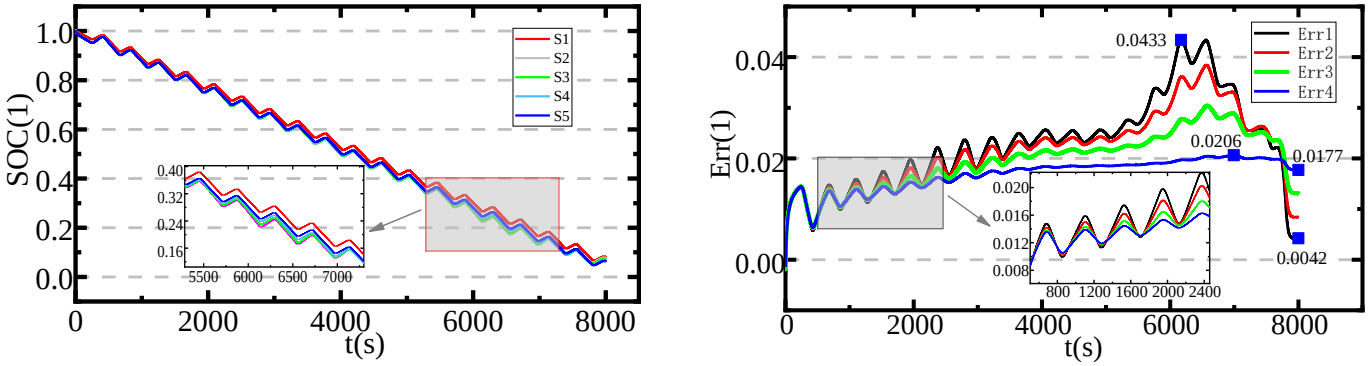

(a) SOC estimation results of different algorithms under DST conditions

(b) SOC estimation error of different algorithms under DST conditions

Figure 12. SOC estimation results and errors of DST condition

Table 3. Comparison of SOC estimation results of different algorithms under BBDST conditions.

Method	MAE	MAX	RMSE
EKF	0.04264	0.04341	0.04231
FFRLS-EKF	0.03153	0.03847	0.03276
AFS-FFRLS-EKF	0.01961	0.03042	0.02036
AFS-FFRLS-DEEKF	0.01684	0.02063	0.01713

In Figure 12(a), S1 indicates the actual SOC value, S2 is the SOC estimation result of the EKF algorithm based on the offline parameter identification of the second-order RC model, S3 represents the EKF algorithm SOC estimation value based on the FFRLS algorithm, and S4 represents the SOC estimation result based on the AFS-FFRLS Algorithm and EKF algorithm SOC estimation value, S5 represents the SOC estimation value based on AFS-FFRLS algorithm and DE-EKF algorithm. In Figure 12(b), Err1, Err2, Err3, Err4, and Err5 are SOC estimation errors matching with the S2~S5 algorithms in Figure 12(a), respectively.

From the SOC estimation curves in Figure 12, it can be seen that the proposed algorithm AFS-FFRLS-DEEKF is closest to the true SOC curve, while the other three algorithms have significant deviations and fluctuations. From the error curves, the first three algorithms show divergence in the second half of the experiment, while the proposed algorithm maintains good convergence as well as high accuracy. In addition,

it can be seen from Table 3 that the method outperforms the three algorithms under the three error indicators, indicating that the proposed algorithm can estimate the SOC curve better with higher accuracy and stability.

3.5 Experimental results of SOC with initial value of 0.8

To further verify the effectiveness of the algorithm, tests were conducted with a non-full charge battery under the above three operating conditions. For all three operating conditions, the actual SOC value is set to 0.8 and the initial SOC value for the other algorithms is set to 0.7. The SOC estimation results are shown in Figure 13.

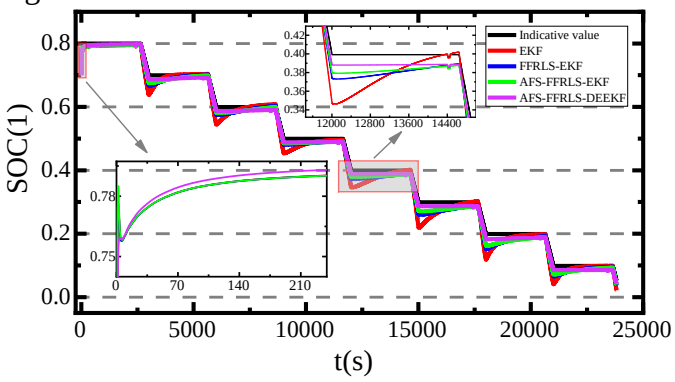

(a) SOC estimation results in 0.8 initial value under HPPC condition

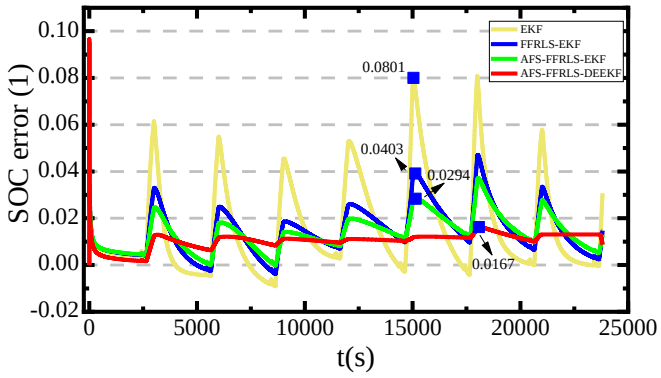

(b) SOC estimation errors in 0.8 initial value under HPPC condition

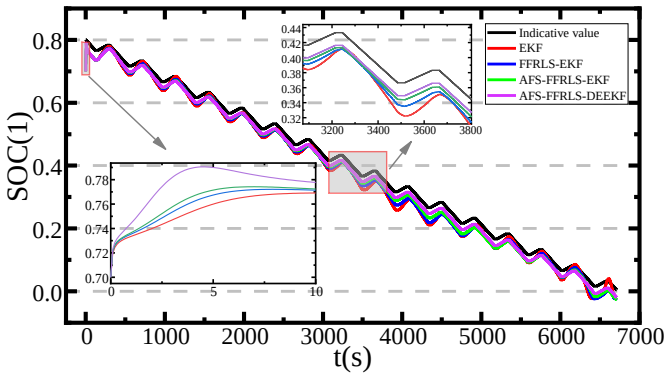

(c) SOC estimation results in 0.8 initial value under DST condition

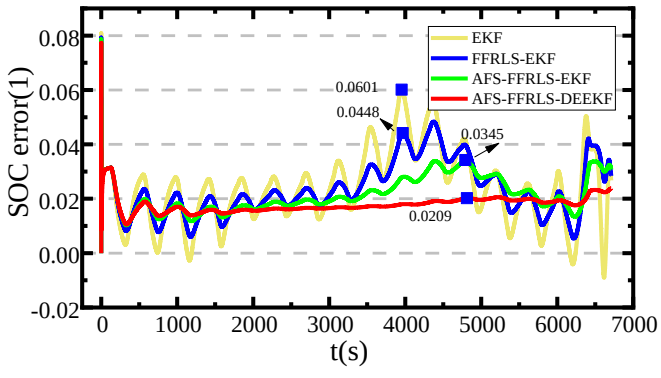

(d) SOC estimation errors in 0.8 initial value under DST condition

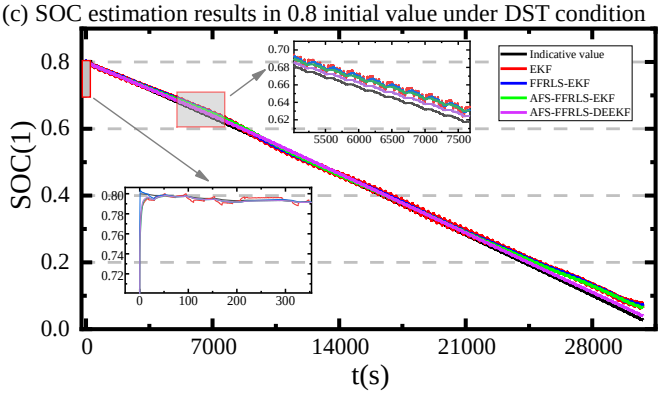

(e) SOC estimation results in 0.8 initial value under BBDST condition

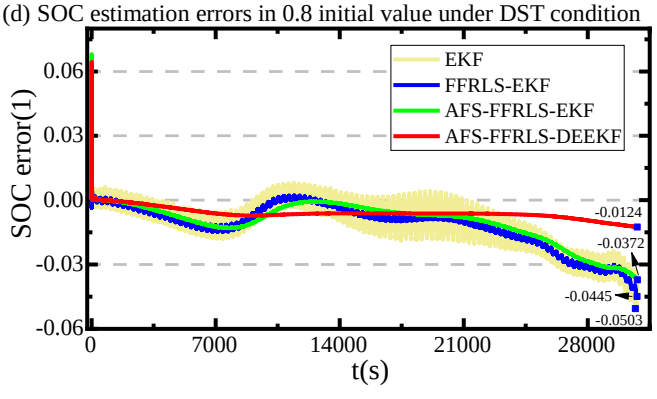

(f) SOC estimation errors in 0.8 initial value under BBDST condition

Figure 13. Results of SOC estimation in 0.8 initial value under different conditions

In Figure 13, it can be seen from the SOC estimation results that the proposed algorithm AFS-FFRLS-DEEKF can quickly correct the estimated route with the best convergence among the four algorithms when the power is not full. A fast convergence speed is important for SOC estimation, and it is equally important

whether the SOC can still be estimated accurately after convergence. The error results show that the proposed algorithm has the lowest error curve fluctuation among the four algorithms, and the error can be stabilized within 2%, 1.5%, and 2% for HPPC, DST, and BBDST conditions, respectively, further verifying the effectiveness and robustness of the proposed algorithm.

3.6 Experimental results of SOC in different algorithms

The data used in this section is from the Battery Research Group at the Center for Advanced Life Cycle Engineering (CALCE) at the University of Maryland. The associated data set can be downloaded by visiting https://web.calce.umd.edu/batteries/data.htm. The INR 18,650–20R cell is selected as the test target. All tests are conducted at 25°C. A basic description of this battery is given in Table 4.

Table 4. Basic specifications of INR 18,650–20R battery.

Capacity Rating	Cell Chemistry	Weight	Dimensions	Length	Nominal voltage	Upper/lower cut-off voltage
2000 mAh	LNMC/Graphite	45.0g	18.33 ± 0.07mm	64.85 ± 0.15mm	3.6V	2.5V/4.2V

To further verify the effectiveness of the proposed algorithm, three advanced algorithms are selected for comparison with the proposed algorithm. The algorithms compared in this section are AEKF [43], MIEKF [44] and AHIF [45] algorithms. For a fairly comparison, the proposed AFSFFRLS algorithm was used for each algorithm's parameter identification method and run 20 times independently, and the comparison is performed under Dynamic stress test (DST), Federal Urban Driving Schedule (FUDS) and Beijing Dynamic Stress Test (BJDST) conditions respectively. The SOC estimation results of the four algorithms are shown in Figure 14.

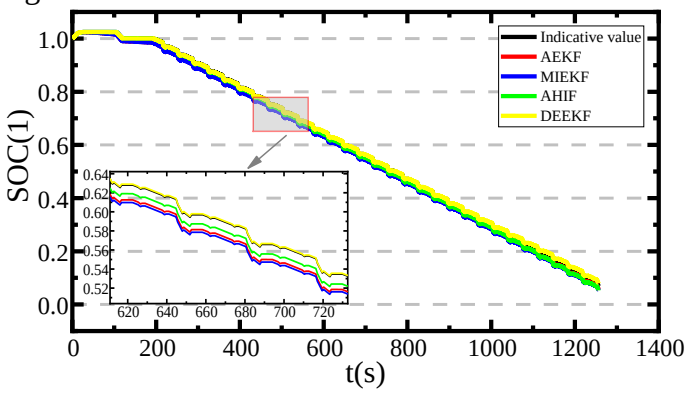

(a) SOC estimation results under DST condition

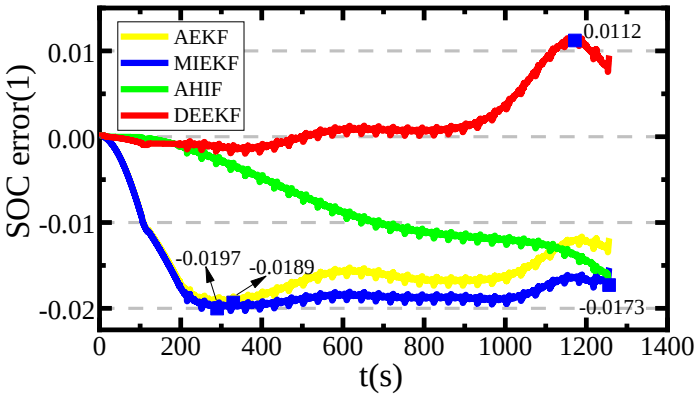

(b) SOC estimation error results under DST condition

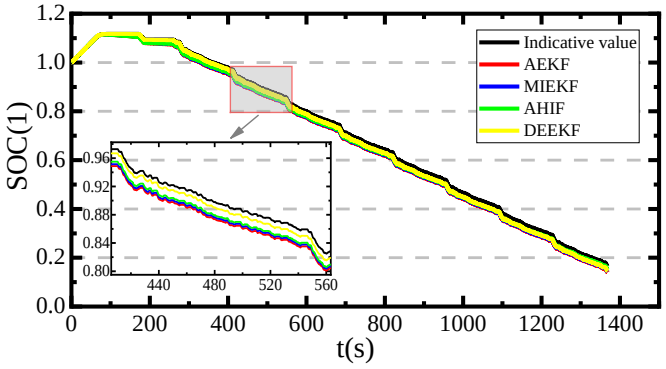

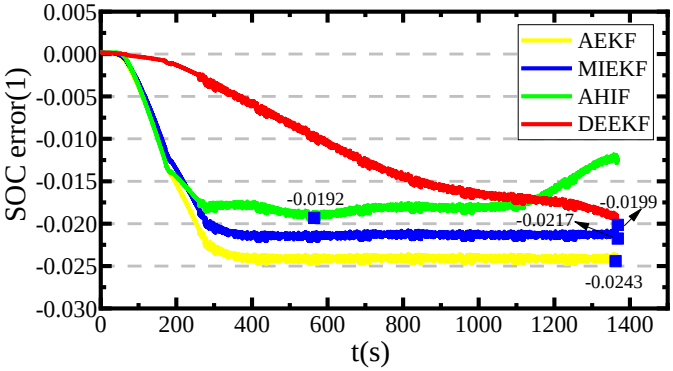

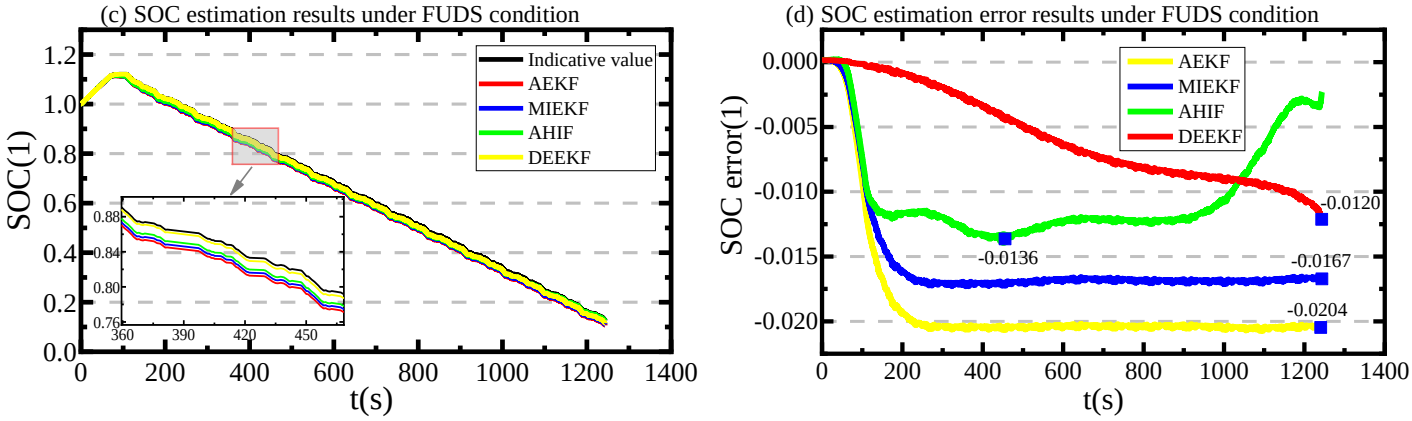

Figure 14. Results of SOC estimation under different conditions

Table 5. Error indicators of different algorithms under different working conditions

Method	DST			FUDS			BJDST		
	MAE	MAX	RMSE	MAE	MAX	RMSE	MAE	MAX	RMSE
AEKF	0.0149	0.0189	0.0155	0.0210	0.0243	0.0221	0.0186	0.0204	0.0193
MIEKF	0.0169	0.0197	0.0175	0.0186	0.0217	0.0196	0.0154	0.0167	0.0160
AHIF	0.0136	0.0173	0.0092	0.0156	0.0192	0.0163	0.0137	0.0136	0.0128
DEEKF	0.0097	0.0112	0.0081	0.0106	0.0199	0.0124	0.0101	0.0120	0.0107

From Table 5, it can be seen that the proposed algorithm DEEKF has the best performance in terms of metrics for the three operating conditions, and the obtained MAE and RMSE values are the smallest. The difference between the four algorithms is not significant, which means that it is effective in the direction of making improvements to the noise. In addition, Figure 14 plots the convergence curves as well as the error curves for each algorithm for 20 independent runs. From the convergence curves, it can be seen that all four algorithms perform well in terms of convergence ability, but there is no doubt that the proposed algorithm DEEKF is the best performer among them. The error curves show that the proposed algorithm is in a smaller error domain, which means that the DEEKF algorithm still performs the best in precision, further validating the effectiveness of the proposed algorithm.

4 Conclusion

In this paper, a new joint AFS-FFRLS-DEEKF algorithm for lithium battery SOC estimation is proposed. Among them, the AFS-FFRLS algorithm completes the task of parameter identification, establishes the objective function with the purpose of minimizing the absolute value of the difference between the actual end-voltage value and the estimated end-voltage value, adjusts the forgetting factor value in real-time, and responds to the parameter identification effect with end-voltage experiments and maps to SOC estimation. The DEEKF algorithm is used for SOC estimation and realizes the process noise dynamics by updating the process noise covariance through the DE algorithm in simulating the actual situation while optimizing the estimation results. The combined experiments compare the joint algorithm with several other algorithms, and the results show that the proposed joint algorithm is effective.

The following findings can be summarized from the overall research process.

1) The AFS-FFRLS algorithm terminal voltage estimation error is stable within 4% and works well for SOC estimation mapping. The joint algorithm stabilizes the SOC estimation error within 1.9%, 2.7% and 2.4% for HPPC, BBDST and DST conditions, respectively, which effectively improves the SOC estimation accuracy.

2) The proposed DEEKF algorithm achieves close to realistic process noise covariance dynamics, and the average error of the proposed algorithm is maintained at about 1% under the three operating conditions provided by the University of Maryland battery group, which is the best performance in comparison with three advanced algorithms, effectively overcoming the effect of process noise and improving the SOC estimation accuracy.

3) In the case of SOC initial value set to 0.8 and algorithm initial value set to 0.7, the joint algorithm AFS-FFRLS-DEEKF can converge quickly and maintain the estimation error within 2% for all three operating conditions, which proves that the joint algorithm has good robustness.

In future work, further improvements will be made to reduce the computation time based on the algorithm structure and algorithm flaws, while considering experiments under different temperatures. Extending its estimation objectives, such as joint estimation of SOC and SOH.

5 Acknowledgement

The work is supported by the National Natural Science Foundation of China (No. 62173281, 61801407).

6 References

[1].Liu, Y. F., J. Q. Li, G. Zhang, B. Hua, and N. Xiong, State of Charge Estimation of Lithium-Ion Batteries Based on Temporal Convolutional Network and Transfer Learning. Ieee Access, 2021. **9**: p. 34177-34187.

[2].Wu, L. X., K. Liu, H. Pang, and J. M. Jin, Online SOC Estimation Based on Simplified Electrochemical Model for Lithium-Ion Batteries Considering Current Bias. Energies, 2021. **14**(17).

[3].Du, B. H., Z. Yu, S. H. Yi, Y. L. He, and Y. L. Luo, State-of-charge estimation for second-life lithium-ion batteries based on cell difference model and adaptive fading unscented Kalman filter algorithm. International Journal of Low-Carbon Technologies, 2021. **16**(3): p. 927-939.

[4].Miao, Y. and Z. Gao, Estimation for state of charge of lithium-ion batteries by adaptive fractional-order unscented Kalman filters. Journal of Energy Storage, 2022. **51**.

[5].He, M. F., S. L. Wang, C. Fernandez, C. M. Vu, X. X. Li, and E. D. Bobobee, A Novel Adaptive Particle Swarm Optimization Algorithm Based High Precision Parameter Identification and State Estimation of Lithium-Ion Battery. International Journal of Electrochemical Science, 2021. **16**(5).

[6].Li, W., Y. Xie, X. S. Hu, Y. J. Zhang, H. H. Li, and X. K. Lin, An Online SOC-SOTD Joint Estimation Algorithm for Pouch Li-Ion Batteries Based on Spatio-Temporal Coupling Correction Method. Ieee Transactions on Power Electronics, 2022. **37**(6): p. 7370-7386.

[7].Jiaqiang, E., B. Zhang, Y. Zeng, M. Wen, K. X. Wei, Z. H. Huang, J. W. Chen, H. Zhu, and Y. W. Deng, Effects analysis on active equalization control of lithium-ion batteries based on intelligent estimation of the state-of-charge. Energy, 2022. **238**.

[8].Ren, Z., C. Q. Du, Z. Y. Wu, J. B. Shao, and W. J. Deng, A comparative study of the influence of different open circuit voltage tests on model-based state of charge estimation for lithium-ion batteries. International Journal of Energy Research, 2021. **45**(9): p. 13692-13711.

[9].Xiao, R. X., Y. W. Hu, X. G. Jia, and G. S. Chen, A novel estimation of state of charge for the lithium-ion battery in electric vehicle without open circuit voltage experiment. Energy, 2022. **243**.

[10].Wang, Y. Q., Y. Cheng, Y. Xiong, and Q. Z. Yan, Estimation of battery open-circuit voltage and state of charge based on dynamic matrix control-extended Kalman filter algorithm. Journal of Energy Storage, 2022. **52**.

[11].Wei, Y. and L. Y. Ling, State-of-Charge Estimation for Lithium-Ion Batteries Based on Temperature-Based Fractional-Order Model and Dual Fractional-Order Kalman Filter. Ieee Access, 2022. **10**: p. 37131-37148.
[12].Zhang, S. Z. and X. W. Zhang, A novel non-experiment-based reconstruction method for the relationship between open-circuit-voltage and state-of-charge/state-of-energy of lithium-ion battery. Electrochimica Acta, 2022. **403**.
[13].Babaeiyazdi, I., A. Rezaei-Zare, and S. Shokrzadeh, State of charge prediction of EV Li-ion batteries using EIS: A machine learning approach. Energy, 2021. **223**.
[14].Xia, Z. Y. and J. A. Abu Qahouq, State-of-Charge Balancing of Lithium-Ion Batteries With State-of-Health Awareness Capability. Ieee Transactions on Industry Applications, 2021. **57**(1): p. 673-684.
[15].Mc Carthy, K., H. Gullapalli, K. M. Ryan, and T. Kennedy, Electrochemical impedance correlation analysis for the estimation of Li-ion battery state of charge, state of health and internal temperature. Journal of Energy Storage, 2022. **50**.
[16].Hannan, M. A., D. N. T. How, M. S. H. Lipu, P. J. Ker, Z. Y. Dong, M. Mansur, and F. Blaabjerg, SOC Estimation of Li-ion Batteries With Learning Rate-Optimized Deep Fully Convolutional Network. Ieee Transactions on Power Electronics, 2021. **36**(7): p. 7349-7353.
[17].Mao, X. J., S. J. Song, and F. Ding, Optimal BP neural network algorithm for state of charge estimation of lithium-ion battery using PSO with Levy flight. Journal of Energy Storage, 2022. **49**.
[18].Li, R., W. R. Li, and H. N. A. Zhang, State of Health and Charge Estimation Based on Adaptive Boosting integrated with particle swarm optimization/support vector machine (AdaBoost-PSO-SVM) Model for Lithium-ion Batteries. International Journal of Electrochemical Science, 2022. **17**(2).
[19].Oyewole, I., A. Chehade, and Y. Kim, A controllable deep transfer learning network with multiple domain adaptation for battery state-of-charge estimation. Applied Energy, 2022. **312**.
[20].Liu, X. T., K. Li, J. Wu, and Y. He, An extended Kalman filter based data-driven method for state of charge estimation of Li-ion batteries. Journal of Energy Storage, 2021. **40**.
[21].Tian, H. X., A. Li, and X. Y. Li, SOC estimation of lithium-ion batteries for electric vehicles based on multimode ensemble SVR. Journal of Power Electronics, 2021. **21**(9): p. 1365-1373.
[22].Adaikkappan, M. and N. Sathiyamoorthy, A real time state of charge estimation using Harris Hawks optimization-based filtering approach for electric vehicle power batteries. International Journal of Energy Research, 2022. **46**(7): p. 9293-9309.
[23].Zhang, F., H. Zhi, P. Zhou, Y. D. Hong, S. Wu, X. Y. Zhao, and C. J. Yang, State of charge estimation of Li-ion battery for underwater vehicles based on EKF-RELM under temperature-varying conditions. Applied Ocean Research, 2021. **114**.
[24].Cui, X. B. and B. W. Xu, State of Charge Estimation of Lithium-Ion Battery Using Robust Kernel Fuzzy Model and Multi-Innovation UKF Algorithm Under Noise. Ieee Transactions on Industrial Electronics, 2022. **69**(11): p. 11121-11131.
[25].Huang, C., X. Y. Yu, Y. C. Wang, Y. Q. Zhou, and R. Li, State of charge estimation of li-ion batteries based on the noise-adaptive interacting multiple model. Energy Reports, 2021. **7**: p. 8152-8161.
[26].Peng, J. K., J. Y. Luo, H. W. He, and B. Lu, An improved state of charge estimation method based on cubature Kalman filter for lithium-ion batteries. Applied Energy, 2019. **253**.
[27].Xia, B. Z., Z. Sun, R. F. Zhang, and Z. Z. Lao, A Cubature Particle Filter Algorithm to Estimate the State of the Charge of Lithium-Ion Batteries Based on a Second-Order Equivalent Circuit Model. Energies, 2017. **10**(4).
[28].Rezaei, O., R. Habibifar, and Z. L. Wang, A Robust Kalman Filter-Based Approach for SoC Estimation of Lithium-Ion Batteries in Smart Homes. Energies, 2022. **15**(10).
[29].Fu, S. Y., W. Liu, W. L. Luo, Z. F. Zhang, M. H. Zhang, L. Wu, C. D. Luo, T. L. Lv, and J. Y. Xie, State of charge estimation of lithium-ion phosphate battery based on weighted multi-innovation cubature Kalman filter. Journal of Energy Storage, 2022. **50**.
[30].Dao, V., M. C. Dinh, C. S. Kim, M. Park, C. H. Doh, J. H. Bae, M. K. Lee, J. Liu, and Z. Bai, Design of an Effective State of Charge Estimation Method for a Lithium-Ion Battery Pack Using Extended Kalman Filter and Artificial Neural Network. Energies, 2021. **14**(9).
[31].Ma, D., K. Gao, Y. T. Mu, Z. Q. Wei, and R. H. Du, An Adaptive Tracking-Extended Kalman Filter for SOC Estimation of Batteries with Model Uncertainty and Sensor Error. Energies, 2022. **15**(10).
[32].Roselyn, J. P., A. Ravi, D. Devaraj, and R. Venkatesan, Optimal SoC Estimation Considering Hysteresis Effect for Effective Battery Management in Shipboard Batteries. Ieee Journal of Emerging and Selected Topics in Power Electronics, 2021. **9**(5): p. 5533-5541.
[33].Vyas, U. B. and V. A. Shah, Differential evolution based regression algorithm for mathematical representation of electrical parameters in lithium-ion battery model. Journal of Energy Storage, 2022. **45**.
[34].Li, J. B., M. Ye, K. P. Gao, X. X. Xu, M. Wei, and S. J. Jiao, Joint estimation of state of charge and state of health for lithium-ion battery based on dual adaptive extended Kalman filter. International Journal of Energy Research, 2021. **45**(9): p. 13307-13322.
[35].Guo, X. W., L. Y. Kang, Y. Yao, Z. Z. Huang, and W. B. Li, Joint Estimation of the Electric Vehicle Power Battery State of Charge Based on the Least Squares Method and the Kalman Filter Algorithm. Energies, 2016. **9**(2).
[36].Qin, S., D. C. Qin, H. X. Wu, T. T. Wang, J. Y. Chen, and P. Z. Wang, State of Charge estimation of lithium-ion power battery based on online parameter identification method and BP neural network. International Journal of Electrochemical Science, 2022. **17**(1): p. 22.
[37].Sakile, R. and U. K. Sinha, Estimation of Lithium-Ion Battery State of Charge for Electric Vehicles Using an Adaptive Joint Algorithm. Advanced Theory and Simulations, 2022. **5**(3): p. 15.
[38].Xu, P. P., J. Q. Li, C. Sun, G. D. Yang, and F. C. Sun, Adaptive State-of-Charge Estimation for Lithium-Ion Batteries by Considering Capacity Degradation. Electronics, 2021. **10**(2): p. 17.
[39].Adaikkappan, M. and N. Sathiyamoorthy, A real time state of charge estimation using Harris Hawks optimization-based filtering approach for electric vehicle power batteries. International Journal of Energy Research: p. 17.

[40].Rzepka, B., S. Bischof, and T. Blank, Implementing an Extended Kalman Filter for SoC Estimation of a Li-Ion Battery with Hysteresis: A Step-by-Step Guide. Energies, 2021. **14**(13).
[41].Qiao, J. L., S. L. Wang, C. M. Yu, W. H. Shi, and C. Fernandez, A novel bias compensation recursive least square-multiple weighted dual extended Kalman filtering method for accurate state-of-charge and state-of-health co-estimation of lithium-ion batteries. International Journal of Circuit Theory and Applications, 2021.
[42].Qian, K. F., X. T. Liu, Y. Q. Wang, X. G. Yu, and B. X. Huang, Modified dual extended Kalman filters for SOC estimation and online parameter identification of lithium-ion battery via modified gray wolf optimizer. Proceedings of the Institution of Mechanical Engineers Part D-Journal of Automobile Engineering, 2021.
[43].Ali, M. U., H. F. Khan, H. Masood, K. D. Kallu, M. M. Ibrahim, A. Zafar, S. Oh, and S. Kim, An adaptive state of charge estimator for lithium-ion batteries. Energy Science & Engineering, 2022. **10**(7): p. 2333-2347.
[44].Gu, T. Y., J. Sheng, Q. H. Fan, and D. Q. Wang, The modified multi-innovation adaptive EKF algorithm for identifying battery SOC. Ionics, 2022. **28**(8): p. 3877-3891.
[45].Liu, Y. Y., S. L. Wang, Y. X. Xie, C. Fernandez, J. S. Qiu, and Y. X. Zhang, A novel adaptive H-infinity filtering method for the accurate SOC estimation of lithium-ion batteries based on optimal forgetting factor selection. International Journal of Circuit Theory and Applications, 2022. **50**(10): p. 3372-3386.